Inhibition of IRE1α kinase increases ferroptosis resistance in triple-negative breast cancer cells

SHUO XU[1] and SI-QI YANG[2]

[1]School of Medicine and Health, Urban Vocational College of Sichuan, Chengdu, Sichuan 610110, P.R. China;
[2]State Key Laboratory of Biotherapy, Sichuan University, Chengdu, Sichuan 610041, P.R. China

Received August 31, 2025; Accepted December 9, 2025

DOI: 10.3892/ol.2026.15483

Abstract. Ferroptosis is a regulated form of cell death that serves a pivotal role in tumor suppression. Whilst the ribonuclease activity of inositol-requiring enzyme 1α (IRE1α) is associated with the regulation of ferroptosis, the potential involvement of its kinase domain in this process remains elusive. Thus, the present study aimed to investigate the specific role of the IRE1α kinase domain in regulating ferroptosis in breast cancer, particularly in the triple-negative breast cancer (TNBC) subtype. To this end, it employed a combination of bioinformatic analysis of clinical datasets, pharmacological inhibition of IRE1α kinase and genetic overexpression models in TNBC cell lines. The present study demonstrated that endoplasmic reticulum to nucleus signaling 1 (*ERN*1; the gene encoding IRE1α) was significantly downregulated in breast cancer compared with that in normal tissues, and that lower *ERN1* levels were associated with a worse prognosis of patients with breast cancer. This association persisted in human epidermal growth factor receptor 2-positive and TNBC subtypes. In TNBC, IRE1α kinase inhibitors (APY29 and sunitinib) markedly inhibited ferroptosis induced by system Xc^- inhibition. Moreover, by constructing overexpression models of wild-type IRE1α (IRE1α-WT) and a kinase-dead mutant (IRE1α-K599A), it was demonstrated that IRE1α-WT overexpression significantly enhanced sensitivity to ferroptosis, whereas the kinase-dead mutant had no significant effect. Mechanistically, IRE1α kinase inhibition upregulated solute carrier family 7 member 11 (also known as xCT) expression and promoted glutathione (GSH) synthesis, thereby suppressing ferroptosis. Collectively, the present study reveals a new function of IRE1α kinase in the regulation of ferroptosis, highlighting the critical regulatory role of the IRE1α kinase-xCT-GSH axis in ferroptosis in TNBC. Thus, IRE1α kinase may have potential as a therapeutic target.

Correspondence to: Dr Shuo Xu, School of Medicine and Health, Urban Vocational College of Sichuan, 351 Honghe Zhong Road, Longquanyi, Chengdu, Sichuan 610110, P.R. China
E-mail: xsmxff@163.com

Key words: inositol-requiring enzyme 1α, ferroptosis, triple-negative breast cancer, solute carrier family 7 member 11, glutathione

Introduction

Ferroptosis, as a novel form of regulated cell death, has emerged as a promising therapeutic target in cancer treatment. It not only effectively suppresses tumor growth, but also reverses cancer cell resistance to conventional therapies (1). The combined application of ferroptosis inducers with standard treatments (such as radiotherapy and immunotherapy) can markedly enhance the antitumor efficacy and reduce the risk of recurrence (2). Notably, despite their strong resistance to traditional therapies, highly aggressive mesenchymal-like cancer cells exhibit exceptional vulnerability to ferroptosis (3). Therefore, targeting ferroptosis may provide new therapeutic opportunities for the treatment of cancer.

Breast cancer is the most common malignant tumor among women worldwide, with an estimated 2.3 million new cases diagnosed in 2022 (4). Among these, TNBC is attracting increasing attention due to its distinct molecular characteristics and high aggressiveness (3). TNBC is characterized by the absence of estrogen receptor, progesterone receptor and human epidermal growth factor receptor 2 (HER2), rendering it insensitive to conventional endocrine therapy (5). Patients with TNBC generally have a poorer prognosis, with a 5-year survival rate of approximately 77%, compared with 93% for hormone receptor-positive breast cancers (6). Moreover, compared with other breast cancer subtypes, TNBC exhibits greater susceptibility to ferroptosis inducers (7). Ferroptosis is currently being investigated as a potential therapeutic approach for breast cancer (3,7). Therefore, exploring the regulatory mechanisms of ferroptosis and identifying novel therapeutic targets may provide more effective treatment strategies for TNBC.

Inositol-requiring enzyme 1α (IRE1α) is an endoplasmic reticulum (ER)-resident protein that serves a crucial role in the unfolded protein response (UPR) (8). It contains both kinase and ribonuclease (RNase) domains and is involved in several pathophysiological processes, including immune responses, cell death regulation and neurodegenerative diseases (9,10). Previous research has reported that the RNase activity of IRE1α enhances the sensitivity of TNBC cells to ferroptosis (11). However, whether the kinase activity of IRE1α

contributes to the regulation of ferroptosis in TNBC remains unclear.

Therefore, the present study aimed to analyze the association between IRE1α and breast cancer progression using existing datasets. Moreover, through pharmacological inhibition and genetic manipulation, the present study aimed to investigate the antitumor effects of IRE1α kinase in TNBC cells and explore its underlying molecular mechanisms of action. The findings of the present study may deepen the current understanding of the role of ferroptosis in TNBC and indicate novel therapeutic targets for future research.

Materials and methods

Reagents and assay kit. Erastin (cat. no. S7242), RAS-selective lethal 3 (RSL3; cat. no. S8155), ML162 (cat. no. S4452), sulfasalazine (SAS; cat. no. S1576), APY29 (cat. no. S6623), sunitinib (cat. no. S7781) and IRE1α kinase-inhibiting RNase attenuator (KIRA6; cat. no. S8658) were purchased from Selleck Chemicals. L-Glutamic acid (glutamate; cat. no. G8415), L-Cystine (cat. no. C7602), L-Methionine (cat. no. M5308) and L-Glutamine (cat. no. G8540) were purchased from Sigma-Aldrich (Merck KGaA). Lipofectamine® 3000 Transfection Reagent (cat. no. L3000015), 0.25% Trypsin-EDTA (cat. no. 25200056), Hank's Balanced Salt Solution (HBSS; cat. no. 14175095), Opti-MEM™ (cat. no. 11058021), cystine-deficient DMEM (cat. no. 21013024), BODIPY™ 581/591 C11 (cat. no. D3861), TRIzol® reagent (cat. no. 15596018) and the SuperScript™ IV First-Strand Synthesis System Kit (cat. no. 18091050) were purchased from Thermo Fisher Scientific, Inc. Unless specified, the rest of the reagents used were purchased from Beyotime Biotechnology.

Cell line and culture conditions. The MDA-MB-231 (cat. no. SCSP-5043), MDA-MB-468 (cat. no. SCSP-5053), 4T1 (cat. no. SCSP-5056) and HT1080 (cat. no. TCHu170) cell lines were purchased from The Cell Bank of Type Culture Collection of The Chinese Academy of Sciences. All cells were cultured under standard conditions in DMEM supplemented with 10% fetal bovine serum (catalog no. SFBE; NATOCOR,) and maintained in a humidified incubator at 37˚C with 5% CO_2. The medium was replaced with fresh medium every 3 days. Upon reaching 80-90% confluency, the cells were passaged using 0.25% trypsin-EDTA solution to maintain optimal growth conditions.

Cell viability assay. The aforementioned cell lines (MDA-MB-231, MDA-MB-468, 4T1 and HT1080) were seeded in 96-well plates (3,000 cells/well). After plating, cells were treated with the indicated compounds (Erastin, RSL3, ML162, SAS, glutamate, APY29, sunitinib and KIRA6) at the concentrations detailed in the corresponding figures. After 24 h of treatment at 37˚C, the culture medium was replaced with a mixture of serum-free medium and Cell Counting Kit-8 reagent (cat. no. 96992; MilliporeSigma) at a 9:1 ratio, followed by incubation at 37˚C for 2 h. Cell viability was assessed by measuring the optical density at 450 nm, and the data were normalized to the control group, as previously described (12).

Assessment of lipid peroxidation with BODIPY and malondialdehyde (MDA). Intracellular lipid reactive oxygen species (ROS) were measured using flow cytometry, as previously described (13). A total of 100,000 MDA-MB-231 cells were seeded per well in a 6-well plate. After 6 h of treatment with the indicated compounds (erastin, 2 μM; SAS, 1 mM; glutamate, 20 mM; APY29, 200 nM) at 37˚C, cells were harvested, washed with PBS and incubated with 1 μM BODIPY 581/591 C11 in serum-free medium for 30 min at 37˚C. Cells were then resuspended in 500 μl HBSS and filtered through a 40-μm cell strainer (BD Biosciences). Flow cytometry analysis was immediately performed using an LSRFortessa instrument (BD Biosciences) with a 488 nm laser. Fluorescence signals from both unoxidized (PE channel) and oxidized (FITC channel) C11 were monitored. The ratio of the mean fluorescence intensity of FITC to PE was calculated. Data analysis was performed using FlowJo v10 software (BD Biosciences).

Cellular MDA levels were assessed using a Lipid Peroxidation Assay Kit (cat. no. ab233471; Abcam), as previously described (14). Briefly, cells were treated with compounds (Erastin, 2 μM; SAS, 1 mM; glutamate, 20 mM; APY29, 200 nM) for 12 h at 37˚C. Samples and the MDA color reagent were added to the wells and incubated for 20 min at room temperature. Following this, the reaction solution was introduced, and the mix was incubated for 60 min at room temperature. The resulting product was subsequently assessed at 695 nm using an absorbance microplate reader.

Intracellular glutathione (GSH) assay. MDA-MB-231, MDA-MB-468, and 4T1 cells were treated with compounds (Erastin, 2 μM; SAS, 1 mM; glutamate, 20 mM; APY29, 200 nM) for 24 h at 37˚C and then harvested. GSH was assayed using the GSH and GSSG Assay Kit (cat. no. S0053; Beyotime Biotechnology), as previously described (15). Briefly, cells were washed with ice-cold PBS, harvested and resuspended in three volumes of Protein Removal Reagent M solution. Cell samples were subjected to two rapid freeze-thaw cycles by alternating between liquid nitrogen and a 37˚C water bath. The corresponding assay reagents were added to the appropriate amount of cell sample. After 25 min, absorbance was measured at 412 nm using a microplate reader. GSH content was then calculated based on a standard curve.

Cystine restriction treatment. The restricted medium was prepared by supplementing glutamine-, methionine- and cystine-deficient DMEM with 4 mM glutamine, 200 μM methionine and 10% fetal bovine serum, as previously described (16). For media with specific cystine concentrations, L-cystine was added to this base restricted medium. Prior to the experiments, cells were washed three times with ice-cold PBS to remove residual cystine and then cultured in the cystine-restricted medium. All subsequent assays, including lipid peroxidation and intracellular GSH measurement, were performed under a cystine-restricted condition of 50 μM.

Western blotting. MDA-MB-231, MDA-MB-468, and 4T1 cells were harvested and washed twice with ice cold PBS. Cells were then lysed on ice using RIPA lysis buffer (cat. no. P0013; Beyotime Biotechnology) containing the protease inhibitor PMSF (cat. no. ST507; Beyotime

Biotechnology). Protein samples were quantified using a BCA protein concentration assay kit (cat. no. P0011; Beyotime Biotechnology). Equal amounts of protein (20 μg per lane) were separated using 4-20% SDS-PAGE and transferred to PVDF membranes using wet blotting. To reduce nonspecific binding, the membranes were blocked with 5% skim milk for 1 h at room temperature, followed by incubation with the corresponding primary antibodies overnight at 4˚C with gentle shaking. The following day, the membranes were washed five times with TBST buffer (containing 0.1% Tween-20) for 5 min each and then incubated with horseradish peroxidase-conjugated secondary antibodies: Goat Anti-Mouse IgG (1:5,000; cat. no. ab205719; Abcam) and Goat Anti-Rabbit IgG (1:5,000; cat. no. ab205718; Abcam) at 30˚C for 2 h. After washing three times with TBST (containing 0.1% Tween-20), the membranes were developed using an enhanced chemiluminescence detection reagent (cat. no. P10300; NCM Biotech, China) and images were captured using a ChemiScope 6100 Chemiluminescence Imaging System (CLiNX Science Instruments Co., Ltd.). Finally, grayscale analysis of target bands was performed using ImageJ software (v1.53a; National Institutes of Health). The primary antibodies used in this experiment were as follows: glutathione peroxidase 4 (GPX4; 1:5,000; cat. no. ab125066; Abcam), acyl-CoA synthetase long chain family member 4 (ACSL4; 1:5,000; cat. no. ab155282; Abcam), IRE1α (1:1,000; cat. no. 3294T; Cell Signaling Technology, Inc.), solute carrier family 7 member 11 (SLC7A11; also known as xCT; 1:1,000; cat. no. 12691T; Cell Signaling Technology, Inc.), and the internal controls β-actin (1:1,000; cat. no. sc-47778; Santa Cruz Biotechnology, Inc.) and GAPDH (1:1,000; cat. no. 2118T; Cell Signaling Technology, Inc.).

Establishment of cell models overexpressing IRE1α wild-type (WT) or kinase-dead mutants. Human IRE1α WT (cat. no. 20744; Addgene, Inc.) and human IRE1α kinase-dead mutants (K599A; cat. no. 20745; Addgene, Inc.) were transfected into MDA-MB-231 cells as previously described (17,18). Lentiviral particles were produced using the second-generation packaging plasmids psPAX2 (cat. no. 12260; Addgene, Inc.) and pMD2.G (cat. no. 12259; Addgene, Inc.). For each transfection, 4 μg of the IRE1α transfer plasmid was combined with 3 μg of the packaging plasmid (psPAX2) and 1 μg of the envelope plasmid (pMD2.G). Specifically, the plasmid mix was diluted in 250 μl Opti-MEM containing 5 μl P3000 reagent, and 10 μl Lipofectamine® 3000 (Invitrogen; Thermo Fisher Scientific, Inc.) was diluted in 250 μl Opti-MEM. The two solutions were mixed, incubated at room temperature for 15 min and then added to the 293T cell (ATCC) culture. Transfected cells were maintained at 37˚C with 5% CO_2 for 48-72 h. The lentiviral supernatant was collected at 24 and 48 h post-transfection, pooled, filtered (0.45 μm), and concentrated. For transduction, MDA-MB-231 cells were infected at a multiplicity of infection (MOI) of 5 in the presence of 8 μg/ml polybrene for 24 h. Stable cell lines were subsequently selected using 2 μg/ml puromycin for 7 days, starting 48 h post-transduction. Following a 5-7 day recovery period, overexpression was verified by western blotting.

Bioinformatic analysis. Bioinformatics analysis was performed using web-based bioinformatics tools. *ERN1* levels in normal and breast cancer samples, as well as the profiles of *ERN1* levels in different molecular subtypes of breast cancer, were analyzed using the online University of ALabama at Birmingham CANcer data analysis Portal (UALCAN) (19) (https://ualcan.path.uab.edu/). The levels of *ERN1* in several malignant tumors were analyzed based on the web tool Gene Expression Profiling Interactive Analysis 2 (20) (http://gepia2.cancer-pku.cn). The online Kaplan-Meier Plotter (21) (http://kmplot.com/analysis) was employed to analyze recurrence-free survival differences between *ERN1*-high and -low groups in both overall breast cancer and HER2-positive subtypes, using the default parameters (probe: 227755_at; cut-off: median) based on its integrated breast cancer gene expression dataset. For TNBC-specific analysis, the GSE21653 dataset (available within the Kaplan-Meier Plotter tool) (22) was selected, applying the 'auto-select best cut-off' function.

RNA extraction, cDNA synthesis and reverse transcription-quantitative PCR (qPCR). MDA-MB-231, MDA-MB-468 and 4T1 cells were treated with APY29 (200 nM) for 24 h at 37˚C and subsequently harvested. Total RNA was isolated using TRIzol reagent. cDNA was synthesized using the SuperScript IV First-Strand Synthesis System with the following protocol: 25˚C for 10 min, 50˚C for 10 min, and 80˚C for 10 min. qPCR was performed using the SsoAdvanced Universal SYBR® Green SuperMix (cat. no. 1725270; Bio-Rad Laboratories, Inc.). The thermocycling conditions were as follows: initial denaturation at 95˚C for 30 sec, followed by 40 cycles of 95˚C for 15 sec and 60˚C for 30 sec. Gene expression was normalized to the endogenous reference gene GAPDH using the $2^{-\Delta\Delta Cq}$ method (23). The results are expressed as fold changes relative to the control group. Primer sequences used for qPCR were as follows (24): xCT forward, 5'-TGTGTGGGGTCCTGTCACTA-3'; xCT reverse, 5'-CAGTAGCTGCAGGGCGTATT-3'; GAPDH forward, 5'-ATGGGGAAGGTGAAGGTCG-3'; and GAPDH reverse, 5'-GGGGTCATTGATGGCAACAATA-3'.

Statistical analysis. All experimental data are presented as mean ± standard error of the mean. Unpaired t-test and one- or two-way ANOVA with Tukey's post hoc test were performed using GraphPad Prism 8.0 software (Dotmatics). $P<0.05$ was considered to indicate a statistically significant difference. All cell culture experiments were independently repeated at least three times to ensure data reproducibility and reliability.

Results

IRE1α is associated with the progression of breast cancer. Previous research reported that the activation of IRE1α can promote breast cancer development (25). The present study thus hypothesized that IRE1α may be pathologically associated with breast cancer and validated this using existing clinical datasets. Using the online tool UALCAN, *ERN1* (which encodes IRE1α) levels were analyzed. The results revealed that *ERN1* expression was significantly downregulated in breast cancer tissues compared with that in normal tissues (Fig. 1A). Notably, the *ERN1* levels were significantly lower in

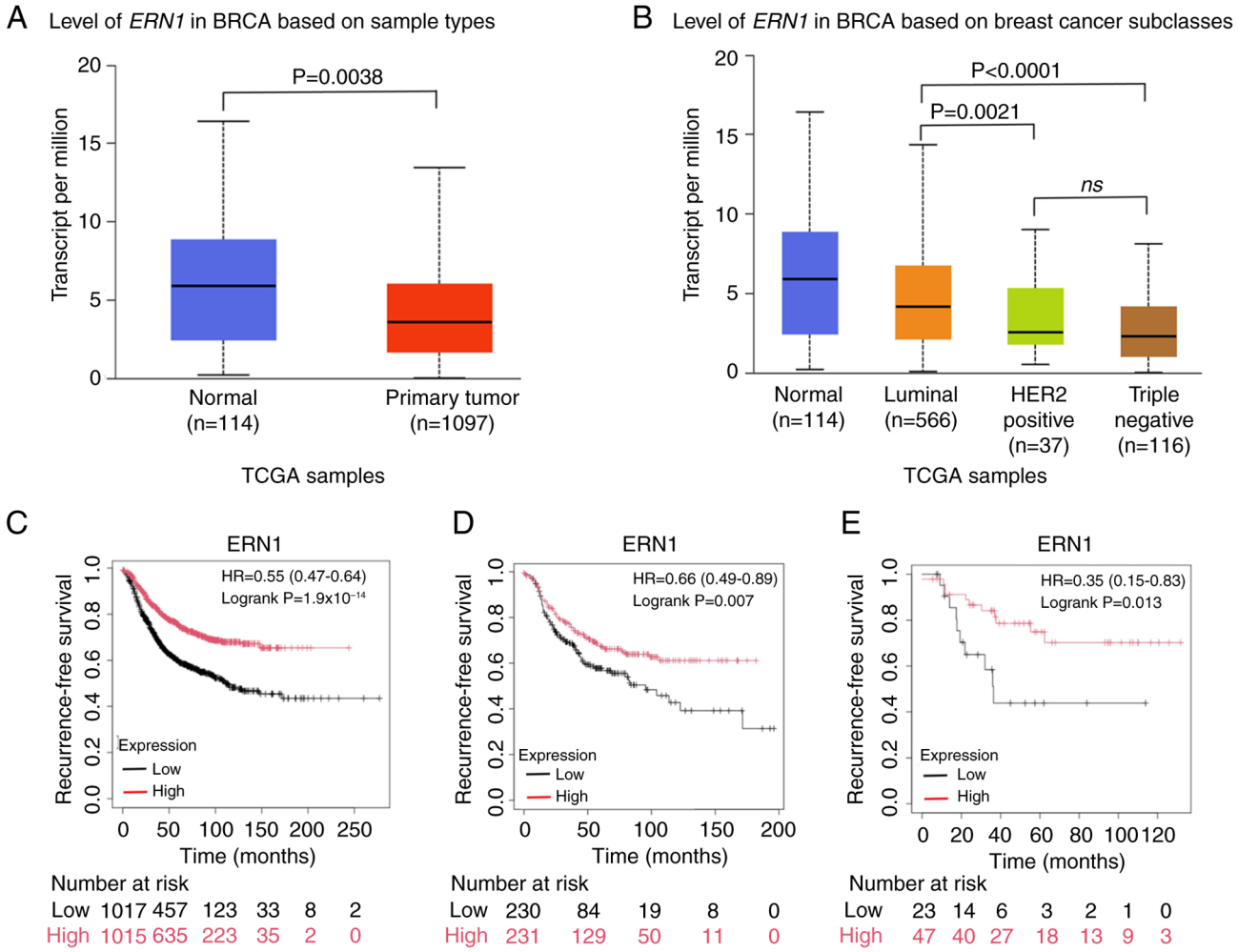

Figure 1. IRE1α is associated with BRCA progression. (A) UALCAN analysis of the level of *ERN1* in BRCA. (B) UALCAN analysis of the level of *ERN1* in BRCA based on BRCA subclasses. The Kaplan-Meier Plotter was used to analyze the outcomes patients with BRCA, and the differences in recurrence-free survival were compared between groups stratified by *ERN1* status: (C) Overall BRCA, (D) HER2-positive breast cancer subset and (E) triple negative BRCA subset. IRE1α, inositol-requiring enzyme 1α; UALCAN, University of ALabama at Birmingham CANcer data analysis Portal; *ERN1*, endoplasmic reticulum to nucleus signaling 1; BRCA, breast cancer; TCGA, The Cancer Genome Atlas; HER2, human epidermal growth factor receptor 2; HR, hazard ratio; ns, not significant.

the more aggressive HER2-positive and TNBC subtypes (26), than in the luminal subtype (Fig. 1B). This suggests that *ERN1* may serve a critical role in the pathological process of HER2-positive and TNBC. Furthermore, pan-cancer analysis further demonstrated that *ERN1* is generally downregulated in multiple cancer types compared with that in normal tissues (Fig. S1). Kaplan-Meier survival analysis also revealed that a low expression of *ERN1* was significantly associated with a worse prognosis of patients with breast cancer (Fig. 1C). In patients who were HER2-positive and in those with TNBC with worse clinical outcomes (27), a lower expression of *ERN1* was also significantly associated a worse prognosis (Fig. 1D and E). Collectively, these findings highlight the potential of targeting IRE1α for breast cancer therapy.

IRE1α kinase pharmacological inhibition confers ferroptosis resistance in TNBC cells. Ferroptosis has emerged as a promising therapeutic target in breast cancer (3), and TNBC exhibits a heightened susceptibility to ferroptosis compared with other molecular subtypes (7). Furthermore, IRE1α possesses both a kinase domain and an RNase domain (8), and whilst previous research has established the involvement of its RNase in modulating ferroptosis sensitivity (11), the potential role of its kinase in ferroptosis regulation remains unexplored. In the present study, to investigate the association between IRE1α kinase and ferroptosis in TNBC, MDA-MB-231 cells were treated with the type I kinase inhibitor APY29 (28) and a dose-effect curve was determined (Fig. S2A). Following subsequent experiments at a non-toxic concentration of APY29 (0.2 μM), it was observed that treatment with APY29 significantly enhanced the resistance of MDA-MB-231 cells to multiple ferroptosis-inducing agents, including erastin, SAS, glutamate and cystine restriction (Fig. 2A-D; P<0.0001 vs. Control at key concentrations). In contrast to the dose-dependent decrease in viability observed with erastin, SAS, and glutamate (which inhibit cystine uptake), cell viability increased with higher cystine concentration in the deprivation assay (Fig. 2D), as cystine itself is a critical substrate for the cellular antioxidant defense against ferroptosis. Notably, these inducers all trigger ferroptosis by directly or indirectly inhibiting system Xc^-, the cystine/glutamate antiporter critical for antioxidant defense (29). This protective effect was further confirmed in

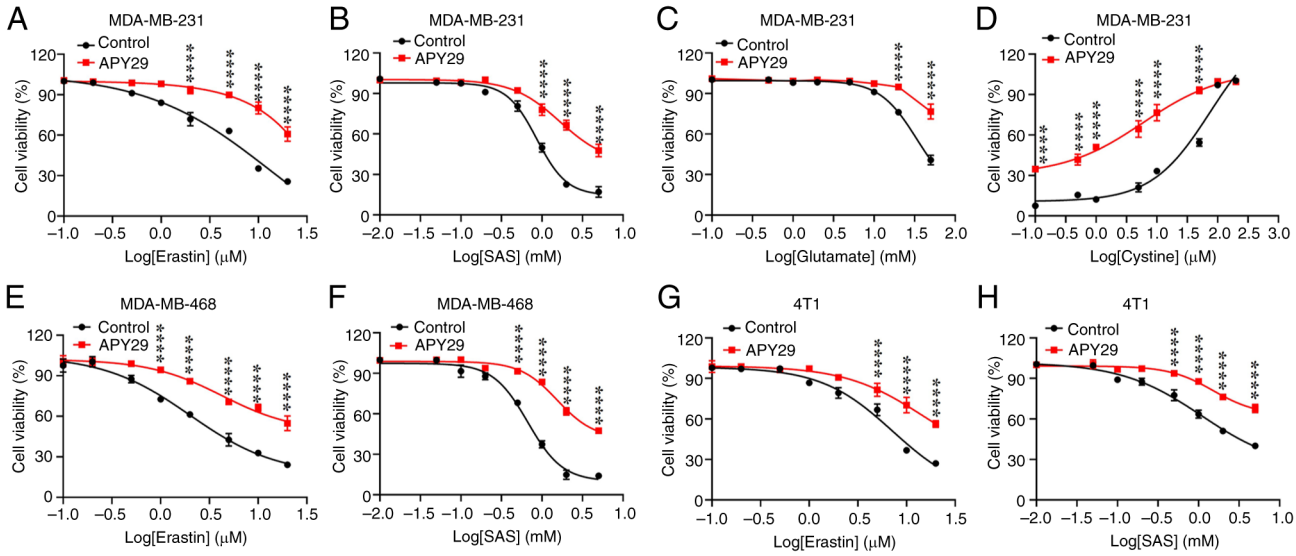

Figure 2. APY29 antagonizes ferroptosis induced by system Xc^- inhibition. Cell viability in MDA-MB-231 cells treated with (A) erastin, (B) SAS, (C) glutamate or (D) cystine restriction for 24 h in the presence or absence of APY29 (0.2 μM). Cell viability in MDA-MB-468 cells treated with (E) erastin or (F) SAS for 24 h in the presence or absence of APY29 (0.2 μM). Cell viability in 4T1 cells treated with (G) erastin or (H) SAS for 24 h in the presence or absence of APY29 (0.2 μM). Data are presented as mean ± standard error of the mean (n=6). ****P<0.0001 vs. Control. SAS, sulfasalazine.

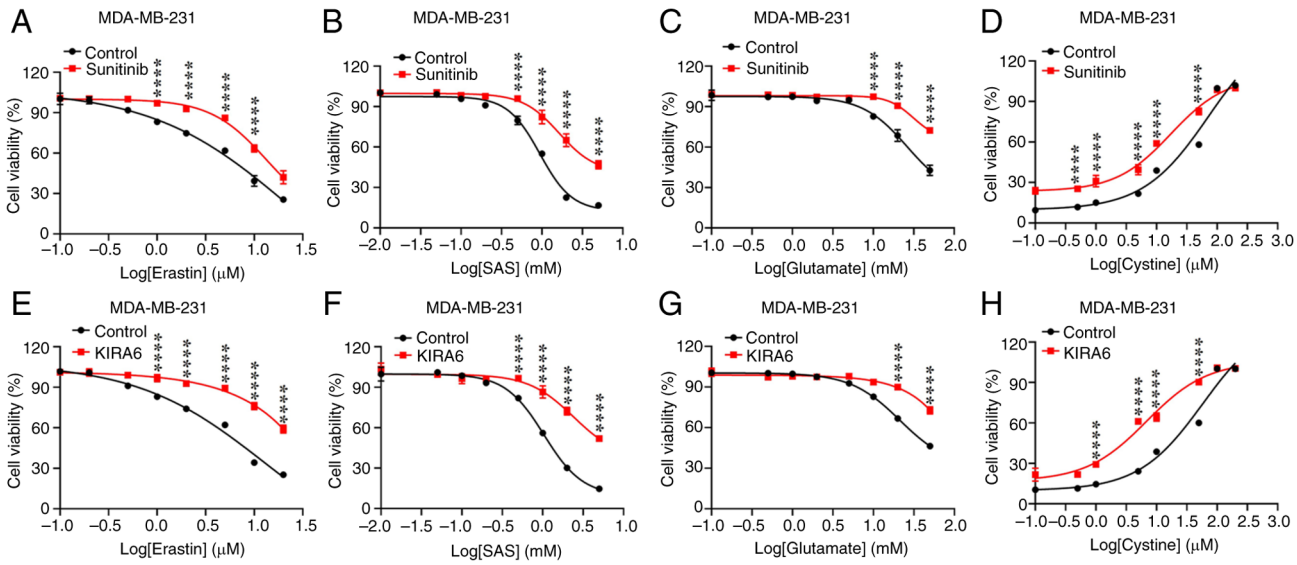

Figure 3. Sunitinib and KIRA6 antagonize ferroptosis induced by system Xc^- inhibition. Cell viability in MDA-MB-231 cells treated with (A) erastin, (B) SAS, (C) glutamate or (D) cystine restriction for 24 h in the presence or absence of sunitinib (0.2 μM). Cell viability in MDA-MB-231 cells treated with (E) erastin, (F) SAS, (G) glutamate or (H) cystine restriction for 24 h in the presence or absence of KIRA6 (0.5 μM). Data are presented as mean ± standard error of the mean (n=6). ****P<0.0001 vs. Control. SAS, sulfasalazine; KIRA6, inositol-requiring enzyme 1α kinase-inhibiting RNase attenuator.

MDA-MB-468 and 4T1 TNBC cells, as well as in HT1080 fibrosarcoma cells (Figs. 2E-H, S2B-D and S3A-D; P<0.0001 vs. Control at key concentrations). Notably, APY29 did not exert a significant effect on ferroptosis induced by the GPX4 inhibitors RSL3 or ML162 (Fig. S3E-H; P>0.05 vs. Control). These results suggest that IRE1α kinase modulates the susceptibility to ferroptosis through the regulation of system Xc^- rather than through GPX4.

The present study further selected two known IRE1α modulators, sunitinib [a type I inhibitor that suppresses IRE1α kinase activity without affecting its RNase function (30)] and KIRA6 [an ATP-competitive IRE1α kinase inhibiting RNase attenuator (31)], for subsequent investigations. First, the cytotoxicity of these compounds was evaluated in MDA-MB-231 cells (Fig. S2E and F). Subsequent experiments were then performed at non-toxic concentrations (sunitinib at 0.2 μM; KIRA6 at 0.5 μM). The results revealed that sunitinib significantly suppressed the ferroptosis induced by erastin, SAS, glutamate or cystine restriction (Fig. 3A-D; P<0.0001 vs. Control at key concentrations). Similarly, KIRA6 exerted marked cytoprotective effects (Fig. 3E-H; P<0.0001 vs. Control at key concentrations). These findings suggest that targeting the IRE1α kinase signaling pathway may represent an effective strategy for modulating ferroptosis.

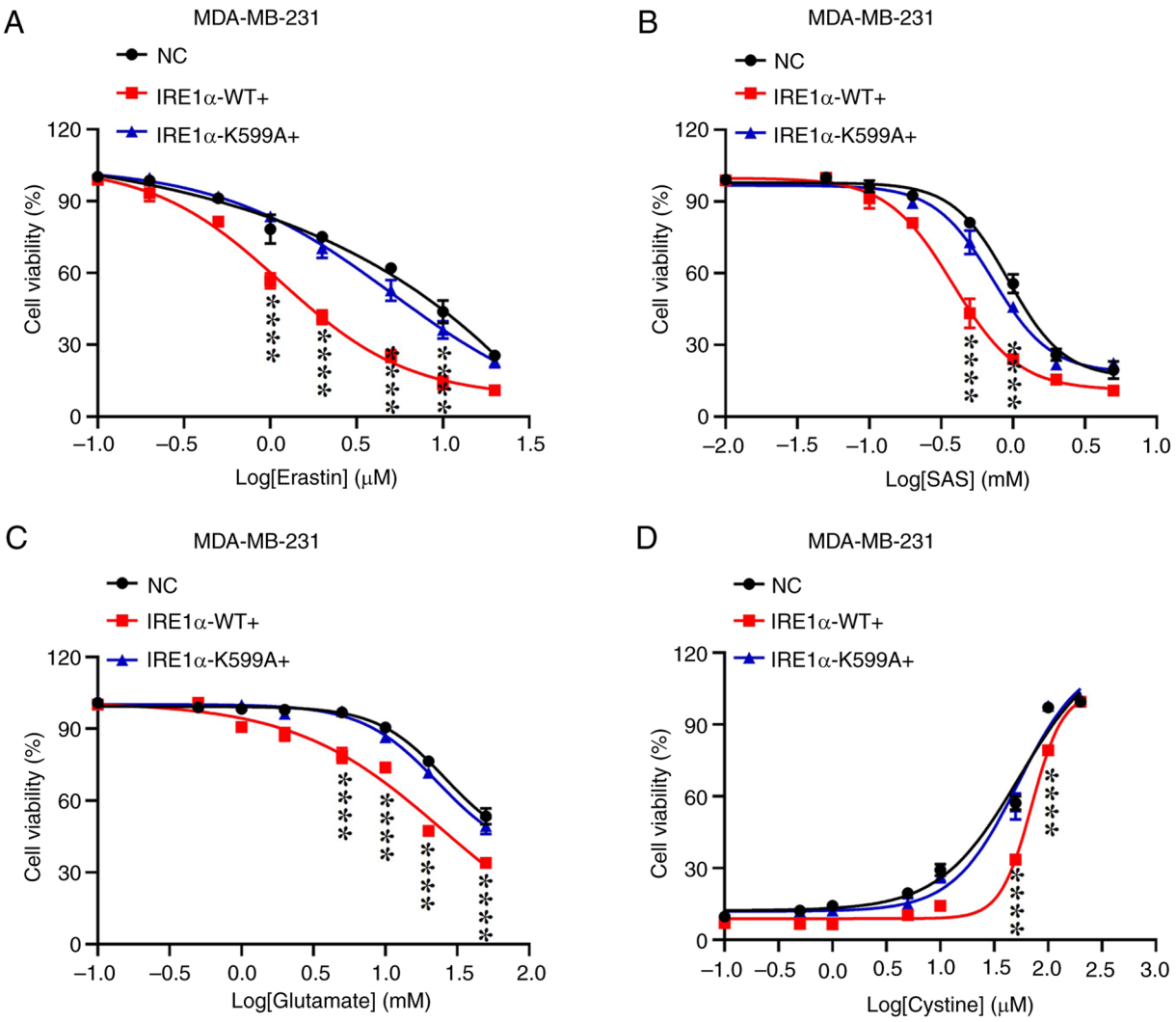

Figure 4. Overexpression of IRE1α-WT promotes ferroptosis. Dose-response of (A) erastin-, (B) SAS-, (C) glutamate- or (D) cystine restriction-induced cytotoxicity in MDA-MB-231 cells overexpressing empty vector, WT IRE1α or kinase-dead IRE1α mutant. Data are presented as mean ± standard error of the mean (n=6). ****P<0.0001 vs. IRE1α-WT+ vs. NC. IRE1α, inositol-requiring enzyme 1α; WT, wildtype; NC, negative control. SAS, sulfasalazine.

Overexpression of IRE1α-WT enhances ferroptosis. To further investigate the role of IRE1α kinase in ferroptosis in MDA-MB-231, the present study established stable cell lines overexpressing either IRE1α-WT or IRE1α-K599A, which abolishes the kinase function of IRE1α (Fig. S4). Subsequent drug resistance assays demonstrated that, compared with the control cells, the overexpression of IRE1α-WT significantly enhanced cellular sensitivity to ferroptosis induced by several stimuli, including erastin, SAS, glutamate and cystine restriction. By contrast, the overexpression of the kinase-dead mutant (IRE1α-K599A) did not exert a significant effect on ferroptosis sensitivity (Fig. 4; P<0.0001 for IRE1α-WT vs. NC, P>0.05 for IRE1α-K599A vs. NC at key concentrations). Taken together, these findings demonstrate that the overexpression of IRE1α-WT, but not the kinase-dead mutant increased the sensitivity of TNBC cells to ferroptosis.

IRE1α kinase inhibition reduces lipid peroxidation. As lipid peroxidation is a critical process in the execution of ferroptosis (3), the present study examined the effects of IRE1α kinase inhibition on MDA [an end product of lipid peroxidation (32)] and lipid ROS levels. The findings demonstrated that treatment with APY29 significantly inhibited the accumulation of MDA (Fig. 5A-D) and lipid ROS (Fig. 5E-H) induced by erastin, SAS, glutamate or cystine restriction (compared with the respective inducer-only groups), whereas IRE1α kinase inhibition with APY29 did not affect the baseline levels of MDA or lipid ROS (compared with the control group) (Fig. 5).

Further investigations revealed that under ferroptosis-inducing conditions, the overexpression of IRE1α-WT significantly increased the accumulation of MDA (Fig. 6A-D) and lipid ROS (Fig. 6E-H) compared with that in the control cells and in cells expressing the kinase-dead mutant. Taken together, these results indicate that the inhibition of IRE1α kinase alleviates lipid peroxidation, thereby suppressing ferroptosis.

Inhibiting IRE1α kinase prevents GSH depletion in ferroptosis. xCT is a key component of system Xc^- and serves a crucial role in regulating intracellular redox homeostasis and determining cellular sensitivity to ferroptosis (1). In the present study, the results revealed that the inhibition of IRE1α kinase

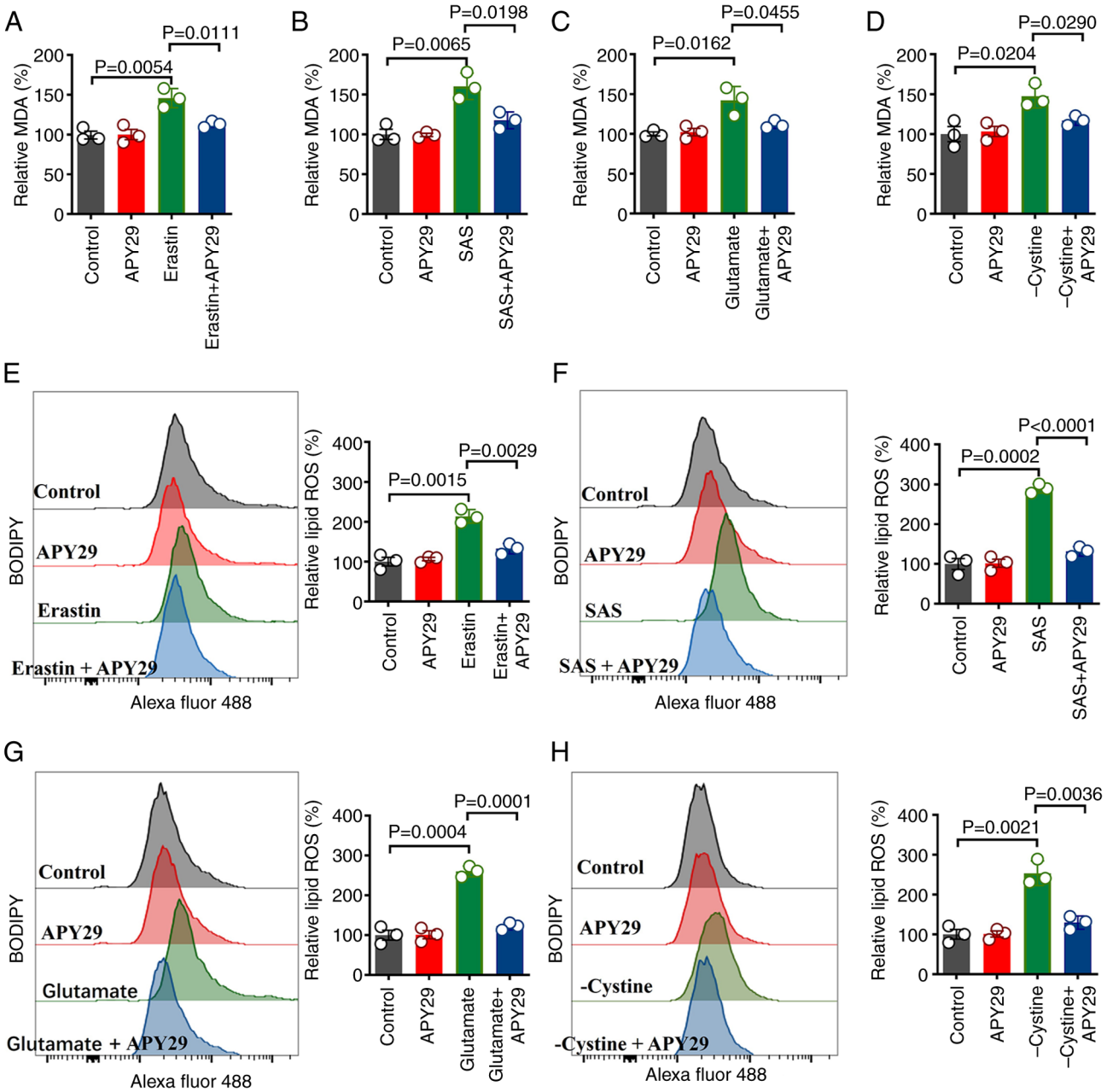

Figure 5. Pharmacological inhibition of IRE1α kinase attenuates lipid peroxidation. MDA levels were measured in MDA-MB-231 cells following 12-h treatment with (A) erastin (5 μM), (B) SAS (1 mM), (C) glutamate (20 mM) or (D) cystine-restricted medium, in the presence or absence of APY29 (0.2 μM). Lipid ROS levels were measured in MDA-MB-231 cells following 6-h treatment with (E) erastin (5 μM), (F) SAS (1 mM), (G) glutamate (20 mM) or (H) cystine-restricted medium, in the presence or absence of APY29 (0.2 μM), with corresponding statistical histograms. Data are presented as mean ± standard error of the mean (n=3). IRE1α, inositol-requiring enzyme 1α; MDA, malondialdehyde; ROS, reactive oxygen species; SAS, sulfasalazine.

activity significantly alleviated ferroptosis induced by system Xc^- suppression (Fig. 2). Specifically, Fig. 2 demonstrates that co-treatment with APY29 markedly improved cell viability compared with cells treated with erastin, SAS, glutamate, or under cystine restriction alone. Thus, it was hypothesized that IRE1α kinase may regulate ferroptosis through xCT. In comparison with controls, treatment of MDA-MB-231 cells with the IRE1α kinase inhibitor, APY29, significantly increased xCT mRNA levels and protein expression (Figs. 7A and S5A). This effect was also observed in MDA-MB-468 (Figs. S5B and S6A) and 4T1 cells (Figs. S5C and S6B). However, the expression of GPX4 and ACSL4, two key ferroptosis regulatory genes (1), remained unaltered (Fig. 7B and C).

The system Xc^- inhibits ferroptosis by maintaining GSH synthesis (33). Further experiments revealed that treatment with APY29 increased baseline GSH levels in MDA-MB-231 cells compared with the untreated control and effectively reversed GSH depletion induced by erastin, SAS, glutamate and cystine restriction compared with the respective inducer-only groups (Fig. 7D-G). This effect was also observed in MDA-MB-468 and 4T1 cells (Fig. S6C-F). Moreover, under these ferroptosis-inducing conditions, the overexpression of wild-type IRE1α significantly reduced GSH levels compared with that in both the control and kinase-dead mutant overexpression groups (Fig. 7H-K). Full original western blot images from Figs. 7 and S6 are presented in Fig. S7. Collectively, the

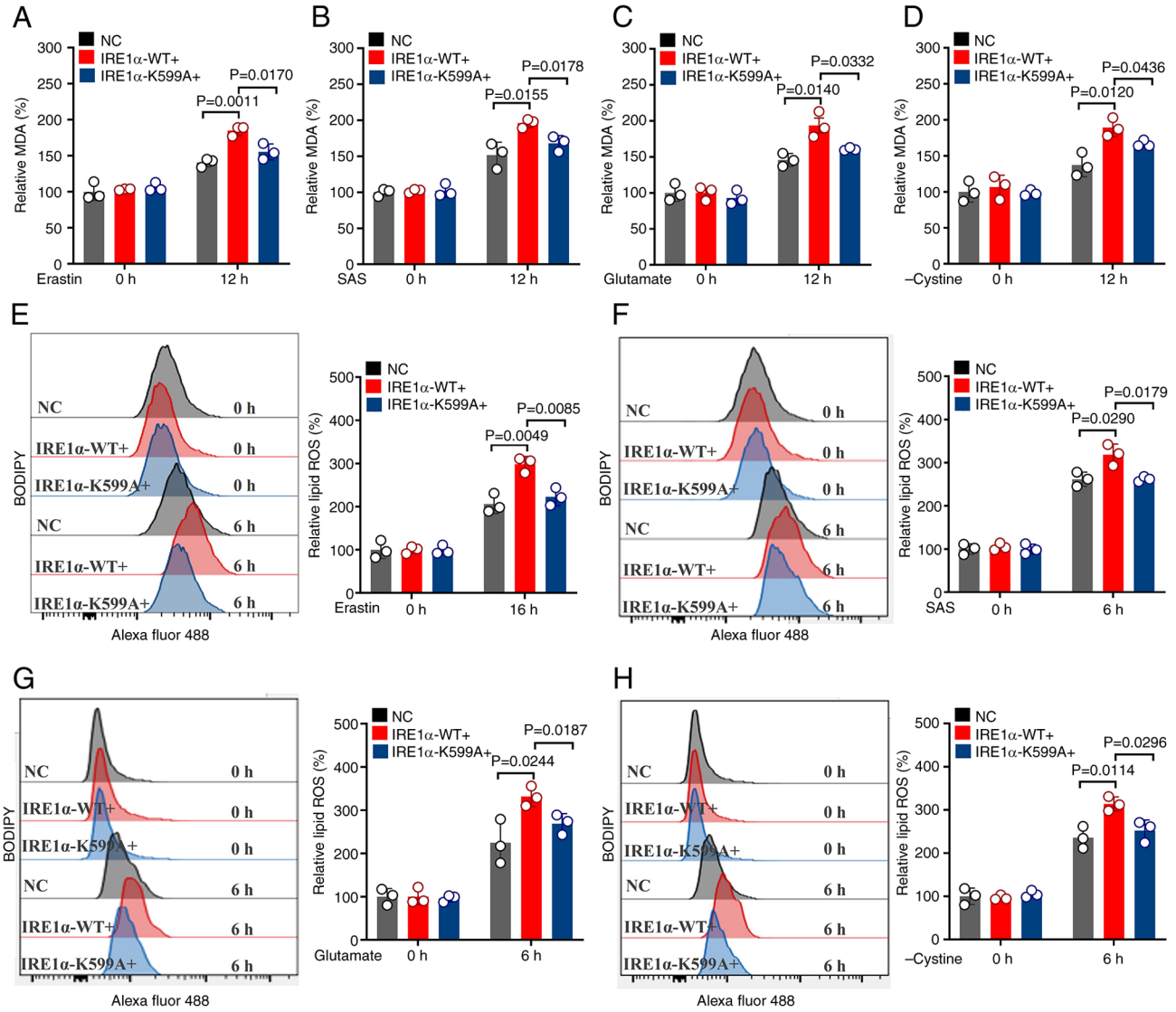

Figure 6. Upregulation of IRE1α kinase increases lipid peroxidation. MDA levels in MDA-MB-231 cells overexpressing empty vector, wild-type IRE1α or kinase-dead IRE1α mutant following 12-h treatment with (A) erastin (5 μM), (B) SAS (1 mM), (C) glutamate (20 mM) or (D) cystine-restricted medium. Lipid ROS levels in MDA-MB-231 cells overexpressing empty vector, wild-type IRE1α or kinase-dead IRE1α mutant following 6-h treatment with (E) erastin (5 μM), (F) SAS (1 mM), (G) glutamate (20 mM) or (H) cystine-restricted medium, with corresponding statistical histograms. Data are presented as mean ± standard error of the mean (n=3). IRE1α, inositol-requiring enzyme 1α; MDA, malondialdehyde; ROS, reactive oxygen species; NC, negative control; WT, wildtype; SAS, sulfasalazine.

aforementioned results indicate that the inhibition of IRE1α kinase activity attenuates GSH depletion, thereby enhancing cellular resistance to ferroptosis.

Discussion

The present study, through the analysis of existing datasets, demonstrated that *ERN1* levels in patients with breast cancer were significantly lower than those in normal samples. Moreover, a low expression of *ERN1* was associated with a poor prognosis of patients with breast cancer. Its low level also predicted a poor prognosis of patients with HER2-positive breast cancer and TNBC. Mechanistically, the inhibition of IRE1α kinase activity upregulated xCT expression and enhanced GSH production, thereby suppressing ferroptosis in TNBC cells. These findings suggest that IRE1α kinase is a potential therapeutic target for TNBC. Notably, similar effects observed in HT1080 cells indicate that this regulatory mechanism may extend to broader cancer therapies.

IRE1α serves multifaceted roles in several types of cancer by modulating the tumor microenvironment, antitumor immunity and chemoresistance (9,34). IRE1α regulates tumor progression through distinct functional domains; small-molecule drugs targeting IRE1α are currently under development as potential anticancer therapeutics (35,36). STF-083010, is a compound specifically targeting the catalytic core of the IRE1α RNase domain that inhibits RNase activity without altering kinase function or the oligomerization state (28). Similarly, 4μ8C selectively inhibits the IRE1α RNase domain, specifically targeting and suppressing regulated IRE1α-dependent decay (RIDD), whilst preserving the kinase activity of IRE1α (37). Previous studies have reported that both these selective IRE1α RNase inhibitors can effectively inhibit the ferroptosis process (11,38). Furthermore,

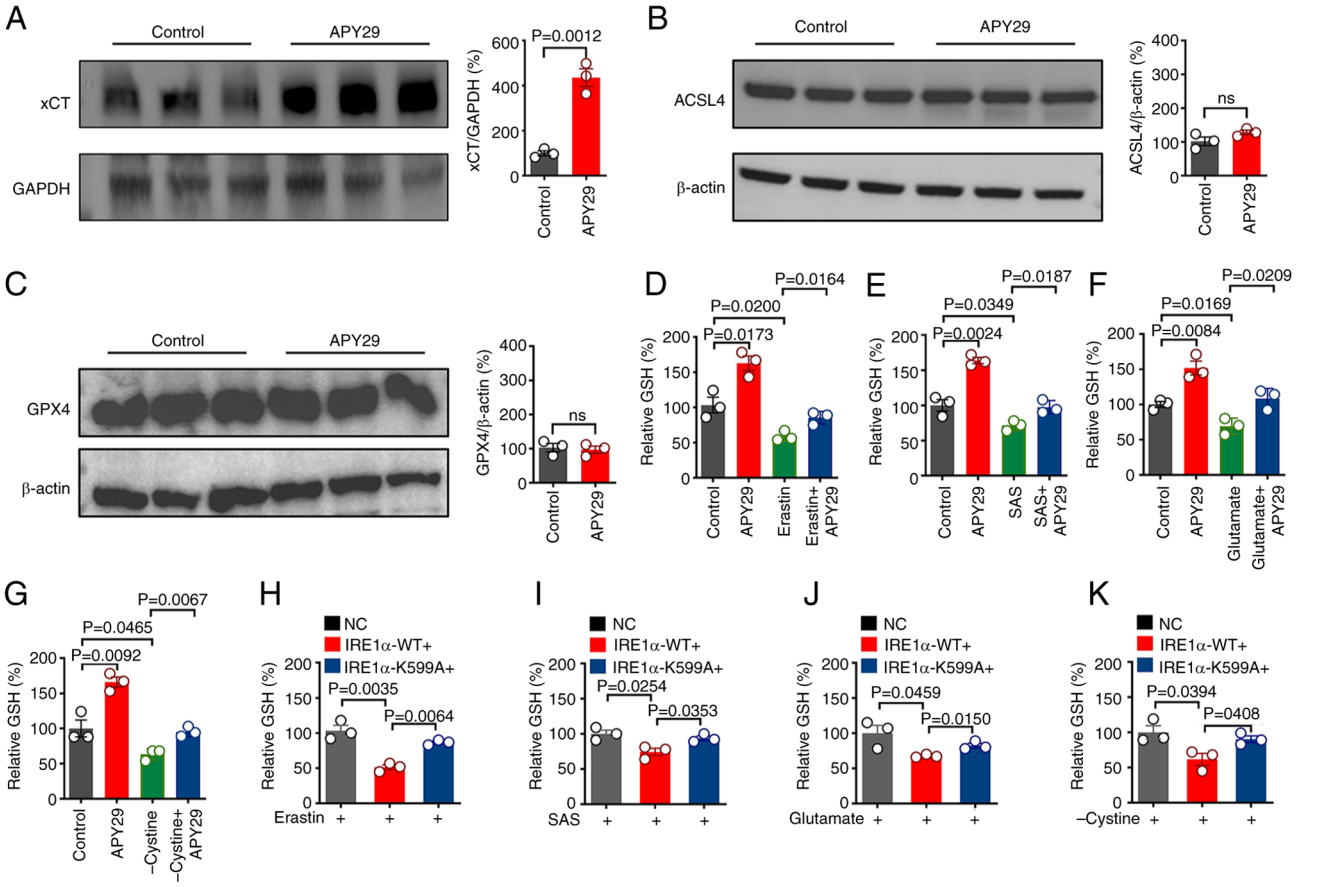

Figure 7. IRE1α regulates GSH and participates in ferroptosis. MDA-MB-231 cells were treated with APY29 (0.2 μM) for 24 h, and the protein expression of (A) xCT, (B) ACSL4 and (C) GPX4 was analyzed using western blotting. GSH levels were measured in MDA-MB-231 cells following 12-h treatment with (D) erastin (5 μM), (E) SAS (1 mM), (F) glutamate (20 mM) or (G) cystine-restricted medium, in the presence or absence of APY29 (0.2 μM). Cellular GSH levels were measured in MDA-MB-231 cells overexpressing empty vector, wild-type IRE1α or the kinase-dead IRE1α mutant following 12-h treatment with (H) erastin (5 μM), (I) SAS (1 mM), (J) glutamate (20 mM) or (K) cystine-restricted medium. Data are presented as mean ± standard error of the mean (n=3). IRE1α, inositol-requiring enzyme 1α; GSH, glutathione; xCT, solute carrier family 7 member 11; ACSL4, acyl-CoA synthetase long chain family member 4; GPX4, glutathione peroxidase 4; NC, negative control; WT, wildtype; ns, not significant; SAS, sulfasalazine.

the present study demonstrated that the IRE1α kinase inhibitors, APY29 and sunitinib [which selectively inhibit IRE1α kinase activity without affecting RNase function (30,39)], effectively rescued the ferroptosis of TNBC cells induced by the inhibitory system Xc^-. This suggests that IRE1α kinase activity is as crucial as its RNase activity in the regulation of ferroptosis. Additionally, KIRA6, a dual inhibitor targeting both the kinase and RNase domains (31), also exhibits ferroptosis-suppressing effects. In summary, the pharmacological modulation of IRE1α provides a promising therapeutic strategy for the treatment of disease by regulating the ferroptosis pathway.

The UPR is a cellular stress response triggered by the accumulation of misfolded proteins in the ER (40). A total of three major pathways mediate the UPR: Protein kinase R-like ER kinase (PERK), activating transcription factor 6 (ATF6) and IRE1α (41). Emerging evidence indicates the crucial role of UPR in regulating the ferroptosis of tumor cells: It has been demonstrated that the loss of PERK function promotes ferroptosis by downregulating xCT in colorectal cancer (42). Moreover, ATF6 exists in two isoforms (α and β), with ATF6α being the predominant form (43). In prostate cancer, ATF6α deficiency has been reported to enhance ferroptotic cell death (44). Additionally, IRE1α contains two functional domains: A kinase domain and an RNase domain (45). Its RNase activity enhances cellular susceptibility to ferroptosis by downregulating xCT expression through the RIDD pathway (11). However, the role of IRE1α kinase in the regulation of ferroptosis remains unclear. The present study demonstrated that the inhibition of IRE1α kinase activity upregulated xCT expression and promoted GSH synthesis, thereby rescuing the ferroptosis of TNBC cells induced by the inhibitory system Xc^-. Notably, although both the kinase and RNase domains can modulate ferroptosis through xCT, these data suggest they may function through independent pathways, as the inhibition of either domain alone is sufficient to confer ferroptosis resistance. To explain this kinase-mediated effect, the present study proposes a model wherein its pharmacological inhibition mimics the functional consequence of IRE1α kinase domain cysteine sulfenylation, which is a redox-sensing modification known to repress its canonical UPR function and activate the NRF2 pathway (46). Therefore, we hypothesize that the observed transcriptional upregulation of SLC7A11 is likely mediated through NRF2 activation. Overall, the findings of the present study unveil a novel role of IRE1α kinase in ferroptosis and provide a more

comprehensive understanding of the function of IRE1α in the ferroptosis pathway.

However, the therapeutic implications of the findings of the present study require careful consideration. The data demonstrate that inhibiting IRE1α kinase activity protects TNBC cells from ferroptosis. This key observation argues against the use of IRE1α kinase inhibitors as a monotherapy, as it would promote tumor survival. Instead, the present work suggests more rational strategies. Firstly, tumors with low IRE1α expression may be intrinsically resistant to ferroptosis inducers, a factor that should be considered in patient stratification. Secondly, a novel combinatorial approach could involve developing IRE1α kinase activators to hypersensitize tumors to ferroptosis inducers, thereby leveraging this axis for therapeutic benefit.

Limitations of the present study should be noted. The findings are primarily based on *in vitro* experiments using a limited set of TNBC cell lines. Future *in vivo* studies and validation in clinical samples are required to confirm the translational relevance of the IRE1α kinase-xCT-GSH axis.

In conclusion, the inhibition of IRE1α kinase activity increases xCT expression and promotes GSH synthesis, a mechanism that serves a critical role in regulating the ferroptosis of TNBC MDA-MB-231 cells. These findings support the IRE1α kinase-xCT-GSH axis as a potential therapeutic strategy for the treatment of TNBC.

Acknowledgements

Not applicable.

Funding

The present work was supported by the Startup Research Fund from Sichuan Urban Vocational College.

Availability of data and materials

The data generated in the present study may be requested from the corresponding author.

Authors' contributions

SX raised funds and contributed to the conception and design of the study. SX and SQY performed the experiments, analyzed the data and wrote the manuscript. SX and SQY confirm authenticity of all the raw data. Both authors read and approved the final manuscript.

Ethics approval and consent to participate

Not applicable.

Patient consent for publication

Not applicable.

Competing interests

The authors declare that they have no competing interests.

References

1. Zhang C, Liu X, Jin S, Chen Y and Guo R: Ferroptosis in cancer therapy: A novel approach to reversing drug resistance. Mol Cancer 21: 47, 2022.
2. Diao J, Jia Y, Dai E, Liu J, Kang R, Tang D, Han L, Zhong Y and Meng L: Ferroptotic therapy in cancer: Benefits, side effects, and risks. Mol Cancer 23: 89, 2024.
3. Xu S, Tuo QZ, Meng J, Wu XL, Li CL and Lei P: Thrombin induces ferroptosis in triple-negative breast cancer through the cPLA2α/ACSL4 signaling pathway. Transl Oncol 39: 101817, 2024.
4. Kim J, Harper A, McCormack V, Sung H, Houssami N, Morgan E, Mutebi M, Garvey G, Soerjomataram I and Fidler-Benaoudia MM: Global patterns and trends in breast cancer incidence and mortality across 185 countries. Nat Med 31: 1154-1162, 2025.
5. Xu T, Ma D, Chen S, Tang R, Yang J, Meng C, Feng Y, Liu L, Wang J, Luo H and Yu K: High GPER expression in triple-negative breast cancer is linked to pro-metastatic pathways and predicts poor patient outcomes. NPJ Breast Cancer 8: 100, 2022.
6. Hsu JY, Chang CJ and Cheng JS: Survival, treatment regimens and medical costs of women newly diagnosed with metastatic triple-negative breast cancer. Sci Rep 12: 729, 2022.
7. Li J, He D, Li S, Xiao J and Zhu Z: Ferroptosis: The emerging player in remodeling triple-negative breast cancer. Front Immunol 14: 1284057, 2023.
8. Raymundo DP, Doultsinos D, Guillory X, Carlesso A, Eriksson LA and Chevet E: Pharmacological targeting of IRE1 in cancer. Trends Cancer 6: 1018-1030, 2020.
9. Unal B, Kuzu OF, Jin Y, Osorio D, Kildal W, Pradhan M, Kung SHY, Oo HZ, Daugaard M, Vendelbo M, *et al*: Targeting IRE1alpha reprograms the tumor microenvironment and enhances anti-tumor immunity in prostate cancer. Nat Commun 15: 8895, 2024.
10. Shi M, Chai Y, Zhang J and Chen X: Endoplasmic reticulum Stress-associated neuronal death and innate immune response in neurological diseases. Front Immunol 12: 794580, 2021.
11. Jiang D, Guo Y, Wang T, Wang L, Yan Y, Xia L, Bam R, Yang Z, Lee H, Iwawaki T, *et al*: IRE1α determines ferroptosis sensitivity through regulation of glutathione synthesis. Nat Commun 15: 4114, 2024.
12. Zheng X, Wei J, Li W, Li X, Wang W, Guo J and Fu Z: PRDX2 removal inhibits the cell cycle and autophagy in colorectal cancer cells. Aging (Albany NY) 12: 16390-16409, 2020.
13. Jiao L, Li X, Luo Y, Wei J, Ding X, Xiong H, Liu X and Lei P: Iron metabolism mediates microglia susceptibility in ferroptosis. Front Cell Neurosci 16: 995084, 2022.
14. Wang X, Chen X, Zhou W, Men H, Bao T, Sun Y, Wang Q, Tan Y, Keller BB, Tong Q, *et al*: Ferroptosis is essential for diabetic cardiomyopathy and is prevented by sulforaphane via AMPK/NRF2 pathways. Acta Pharm Sin B 12: 708-722, 2022.
15. Huang H, Zhang S, Li Y, Liu Z, Mi L, Cai Y, Wang X, Chen L, Ran H, Xiao D, *et al*: Suppression of mitochondrial ROS by prohibitin drives glioblastoma progression and therapeutic resistance. Nat Commun 12: 3720, 2021.
16. Yang X, Wang Z, Samovich SN, Kapralov AA, Amoscato AA, Tyurin VA, Dar HH, Li Z, Duan S, Kon N, *et al*: PHLDA2-mediated phosphatidic acid peroxidation triggers a distinct ferroptotic response during tumor suppression. Cell Metab 36: 762-777.e9, 2024.
17. Chen L, Zhao X, Sheng R, Lazarovici P and Zheng W: Artemisinin alleviates astrocyte overactivation and neuroinflammation by modulating the IRE1/NF-κB signaling pathway in in vitro and in vivo Alzheimer's disease models. Free Radic Biol Med 229: 96-110, 2025.
18. Sanese P, Fasano C, Buscemi G, Bottino C, Corbetta S, Fabini E, Silvestri V, Valentini V, Disciglio V, Forte G, *et al*: Targeting SMYD3 to sensitize homologous Recombination-proficient tumors to PARP-Mediated synthetic lethality. iScience 23: 101604, 2020.
19. Chandrashekar DS, Karthikeyan SK, Korla PK, Patel H, Shovon AR, Athar M, Netto GJ, Qin ZS, Kumar S, Manne U, *et al*: UALCAN: An update to the integrated cancer data analysis platform. Neoplasia 25: 18-27, 2022.
20. Tang Z, Li C, Kang B, Gao G, Li C and Zhang Z: GEPIA: A web server for cancer and normal gene expression profiling and interactive analyses. Nucleic Acids Res 45: W98-W102, 2017.

21. Gyorffy B, Lanczky A, Eklund AC, Denkert C, Budczies J, Li Q and Szallasi Z: An online survival analysis tool to rapidly assess the effect of 22,277 genes on breast cancer prognosis using microarray data of 1,809 patients. Breast Cancer Res Treat 123: 725-731, 2010.
22. Sabatier R, Finetti P, Adelaide J, Guille A, Borg JP, Chaffanet M, Lane L, Birnbaum D and Bertucci F: Down-regulation of ECRG4, a candidate tumor suppressor gene, in human breast cancer. PLoS One 6: e27656, 2011.
23. Livak KJ and Schmittgen TD: Analysis of relative gene expression data using real-time quantitative PCR and the 2(-Delta Delta C(T)) method. Methods 25: 402-408, 2001.
24. Zhang W, Sun Y, Bai L, Zhi L, Yang Y, Zhao Q, Chen C, Qi Y, Gao W, He W, *et al*: RBMS1 regulates lung cancer ferroptosis through translational control of SLC7A11. J Clin Invest 131: e152067, 2021.
25. Wang X, Wang Q, Wang H, Cai G, An Y, Liu P, Zhou H, Chen HW, Ji S, Ye J, *et al*: Small protein ERSP encoded by LINC02870 promotes triple negative breast cancer progression via IRE1α/XBP1s activation. Cell Death Differ 32: 1014-1025, 2025.
26. Alanko J, Tanner M, Vanninen R, Auvinen A and Isola J: Triple-negative and HER2-positive breast cancers found by mammography screening show excellent prognosis. Breast Cancer Res Treat 187: 267-274, 2021.
27. Hoeferlin LA, C EC and Park MA: Challenges in the treatment of triple negative and HER2-Overexpressing breast cancer. J Surg Sci 1: 3-7, 2013.
28. Park H, Shin DH, Sim JR, Aum S and Lee MG: IRE1α kinase-mediated unconventional protein secretion rescues misfolded CFTR and pendrin. Sci Adv 6: eaax9914, 2020.
29. Jiang Y and Sun M: SLC7A11: The Achilles heel of tumor? Front Immunol 15: 1438807, 2024.
30. Makhov P, Naito S, Haifler M, Kutikov A, Boumber Y, Uzzo RG and Kolenko VM: The convergent roles of NF-κB and ER stress in sunitinib-mediated expression of pro-tumorigenic cytokines and refractory phenotype in renal cell carcinoma. Cell Death Dis 9: 374, 2018.
31. Tang X, Teder T, Samuelsson B and Haeggstrom JZ: The IRE1α Inhibitor KIRA6 blocks leukotriene biosynthesis in human phagocytes. Front Pharmacol 13: 806240, 2022.
32. Gawel S, Wardas M, Niedworok E and Wardas P: Malondialdehyde (MDA) as a lipid peroxidation marker. Wiad Lek 57: 453-455, 2004 (In Polish).
33. Koppula P, Zhuang L and Gan B: Cystine transporter SLC7A11/xCT in cancer: Ferroptosis, nutrient dependency, and cancer therapy. Protein Cell 12: 599-620, 2021.
34. Xu L, Peng F, Luo Q, Ding Y, Yuan F, Zheng L, He W, Zhang SS, Fu X, Liu J, *et al*: IRE1α silences dsRNA to prevent taxane-induced pyroptosis in triple-negative breast cancer. Cell 187: 7248-7266.e34, 2024.
35. Harnoss JM, Le Thomas A, Shemorry A, Marsters SA, Lawrence DA, Lu M, Chen YA, Qing J, Totpal K, Kan D, *et al*: Disruption of IRE1α through its kinase domain attenuates multiple myeloma. Proc Natl Acad Sci USA 116: 16420-16429, 2019.
36. Abbasi S, Rivand H, Eshaghi F, Moosavi MA, Amanpour S, McDermott MF and Rahmati M: Inhibition of IRE1 RNase activity modulates tumor cell progression and enhances the response to chemotherapy in colorectal cancer. Med Oncol 40: 247, 2023.
37. Cross BC, Bond PJ, Sadowski PG, Jha BK, Zak J, Goodman JM, Silverman RH, Neubert TA, Baxendale IR, Ron D, *et al*: The molecular basis for selective inhibition of unconventional mRNA splicing by an IRE1-binding small molecule. Proc Natl Acad Sci USA 109: E869-E878, 2012.
38. Chan KY, Yu Y, Kong Y, Cheng L, Yao R, Yin Chair PS, Wang P, Wang R, Sun WY, He RR, *et al*: GPX4-dependent ferroptosis sensitivity is a fitness trade-off for cell enlargement. iScience 28: 112363, 2025.
39. Li C, Tan YP, Gao D, Su R, Xu K, Liu SC, Li XF, Lu YH, Yi LT, Wang G, *et al*: IRE1alpha RNase activity is critical for early embryo development by degrading maternal transcripts. Nucleic Acids Res 53: gkaf520, 2025.
40. Read A and Schroder M: The unfolded protein response: An overview. Biology (Basel) 10: 384, 2021.
41. Kim P: Understanding the unfolded protein response (UPR) pathway: Insights into neuropsychiatric disorders and therapeutic potentials. Biomol Ther (Seoul) 32: 183-191, 2024.
42. Saini KK, Chaturvedi P, Sinha A, Singh MP, Khan MA, Verma A, Nengroo MA, Satrusal SR, Meena S, Singh A, *et al*: Loss of PERK function promotes ferroptosis by downregulating SLC7A11 (System Xc^-) in colorectal cancer. Redox Biol 65: 102833, 2023.
43. Oka OB, van Lith M, Rudolf J, Tungkum W, Pringle MA and Bulleid NJ: ERp18 regulates activation of ATF6alpha during unfolded protein response. EMBO J 38: e100990, 2019.
44. Zhao R, Lv Y, Feng T, Zhang R, Ge L, Pan J, Han B, Song G and Wang L: ATF6α promotes prostate cancer progression by enhancing PLA2G4A-mediated arachidonic acid metabolism and protecting tumor cells against ferroptosis. Prostate 82: 617-629, 2022.
45. Ghosh R, Wang L, Wang ES, Perera BG, Igbaria A, Morita S, Prado K, Thamsen M, Caswell D, Macias H, *et al*: Allosteric inhibition of the IRE1α RNase preserves cell viability and function during endoplasmic reticulum stress. Cell 158: 534-548, 2014.
46. Hourihan JM, Moronetti Mazzeo LE, Fernandez-Cardenas LP and Blackwell TK: Cysteine sulfenylation directs IRE-1 to activate the SKN-1/Nrf2 antioxidant response. Mol Cell 63: 553-566, 2016.